Complete set of deuteron analyzing powers from d[over⃗]p elastic scattering at 190 MeV/nucleon

K. Sekiguchi *et al.*

Phys. Rev. C **96**, 064001 — Published 6 December 2017

DOI: 10.1103/PhysRevC.96.064001

Complete Set of Deuteron Analyzing Powers from $\vec{d}\,p$ Elastic Scattering at 190 MeV/nucleon

K. Sekiguchi[1],* H. Witała[2], T. Akieda[1], D. Eto[1], H. Kon[1], Y. Wada[1], A. Watanabe[1], S. Chebotaryov[3], M. Dozono[4], J. Golak[2], H. Kamada[5], S. Kawakami[6], Y. Kubota[4], Y. Maeda[6], K. Miki[1], E. Milman[3], A. Ohkura[7], H. Sakai[8], S. Sakaguchi[7], N. Sakamoto[8], M. Sasano[8], Y. Shindo[7], R. Skibiński[2], H. Suzuki[8], M. Tabata[7], T. Uesaka[8], T. Wakasa[7], K. Yako[4], T. Yamamoto[6], Y. Yanagisawa[8], and J. Yasuda[7]

[1]*Department of Physics, Tohoku University, Sendai, 980-8578, Japan*
[2]*M. Smoluchowski Institute of Physics, Jagiellonian University, PL-30-348 Cracow, Poland*
[3]*Department of Physics, Kyungpook National University, Daegu 702-701, Korea*
[4]*Center for Nuclear Study, University of Tokyo, Tokyo, 113-0033, Japan*
[5]*Department of Physics, Kyushu Institute of Technology, Kitakyushu 804-8550, Japan*
[6]*Faculty of Engineering, University of Miyazaki, Miyazaki, 889-2192, Japan*
[7]*Department of Physics, Kyushu University, Fukuoka, 819-0395, Japan and*
[8]*RIKEN Nishina Center, Wako, 351-0198, Japan*

(Dated: October 30, 2017)

All deuteron analyzing powers for elastic deuteron–proton (dp) scattering have been measured with a polarized deuteron beam at 186.6 MeV/nucleon. They are compared with results of three-nucleon Faddeev calculations based on the standard, high precision nucleon–nucleon (NN) potentials alone or combined with commonly used three-nucleon force ($3N$F) models such as the Tucson-Melbourne'99 or the Urbana IX. Predicted $3N$F effects localized at backward angles are supported only partially by the data. The data are also compared to predictions based on locally regularized chiral NN potentials. An estimation of theoretical truncation uncertainties in the consecutive orders of chiral expansion suggests that the observed discrepancies between this modern theory and the data could probably be explained including chiral $3N$F's in future calculations. A systematic comparison to the deuteron analyzing power data previously taken at incident energies from 70 to 294 MeV/nucleon clearly shows that not only the cross section but also the analyzing powers reveal growing $3N$F effects when the three-nucleon system energy is increased.

PACS numbers: 21.30.-x, 21.45.-v, 24.10.-i, 24.70.+s

I. INTRODUCTION

One of the main interests of nuclear physics is to understand the forces acting between nuclear constituents. Recently importance of the three-nucleon force ($3N$F) in the nuclear Hamiltonian has been studied in few-nucleon systems as well as in many-nucleon systems [1–3]. Three-nucleon ($3N$) systems, where numerically exact solutions of the corresponding Faddeev equations for any two- and three-nucleon forces are feasible, play an especially important role in these investigations.

Nucleon–deuteron (Nd) scattering offers a good opportunity to study dynamical aspects of $3N$Fs, that are momentum, spin and isospin dependences, since it provides not only cross sections but also a variety of spin observables at different incident nucleon energies. The last two decades have witnessed the extensive experimental and theoretical investigations of the Nd scattering performed in a wide range of incoming nucleon energies up to $E \sim 300$ MeV/nucleon (MeV/N). Theoretical progress made it possible to perform rigorous numerical Faddeev calculations of the $3N$ scattering using the new generation of semi-phenomenological NN interactions such as the AV18 [4], the CDBonn [5] or the Nijmegen 1 and 2 [6] potentials, which describe existing two-nucleon ($2N$) data with very high precision up to 350 MeV. Incorporating in these calculations the 2π-exchange $3N$F models such as the Tucson-Melbourne 99 (TM99) [7] or the Urbana IX [8] have provided clear signatures that the $3N$Fs play an important role in the $3N$ Hamiltonian [9–12]. Experimentally the developments in technology of highly polarized proton and deuteron ion sources as well as their application in recently constructed accelerators, together with sophisticated techniques of target polarization, and constructions of high precision polarimeters have made it possible to get precise data not only for the cross section but also for the spin observables up to $E \sim 300$ MeV/N [13–33]. The experimental success of obtaining high precision data for the Nd scattering together with the theoretical achievements have made this process

*Electronic address: kimiko@lambda.phys.tohoku.ac.jp

a solid testing ground for modern nuclear forces.

The evidence of strong $3N$F effects in the Nd scattering came first from a study of the neutron-deuteron (nd) total cross section [10, 11] and elastic scattering angular distribution [9]. Starting at incoming nucleon energies above $\approx$ 60 MeV theoretical predictions obtained with NN potentials only tend to clearly underestimate the data. The deviation between data and the predictions based on the NN forces only, grows rapidly with the incident energy. Including the TM99 or the Urbana IX $3N$F's, with parameters adjusted to reproduce the ^{3}H and ^{3}He binding energies, allows one to achieve an agreement between theory and data for both Nd elastic scattering and the nd total cross sections up to $\approx$ 130 MeV. However, contrary to the results obtained at these lower energies, for higher incident energies the discrepancies between the data and the calculations are only partially reduced even including the $3N$Fs. In order to exclude the possibility that relativistic effects could be responsible for those higher energy discrepancies, the nonrelativistic $3N$ Faddeev equations were reformulated to include basic relativistic features such as the proper relativistic energy-momentum relation, relativistic NN interactions with their proper boosts and Wigner spin rotations [34, 35]. It turned out that effects of relativity are practically negligible for the elastic scattering differential cross section and spin observables as well as for the total nd cross section. Thus the higher energy discrepancies between theory and data must result from short-range $3N$F components, which become active at higher energies.

Also for spin observables in elastic Nd scattering a complex pattern of discrepancies between theory and data has been found. For some spin observables effects of $3N$F's depend on whether the AV18 NN potential is combined with the TM99 or with the Urbana IX 3NF interaction [12]. It may indicate possible inconsistencies between NN potentials and $3N$F models commonly used in $3N$ calculations.

These inconsistencies can be cured in the chiral effective field theory (EFT) approach, which allows one to derive consistent nuclear forces acting in many-nucleon systems. It provides consistent NN- and $3N$- forces in a systematically improvable way - order by order in chiral expansion, starting from the leading order (LO). Accurate NN potentials at N^{3}LO have been available for about a decade [36, 37] and $3N$F's, starting at N^{2}LO [38], have been derived up to N^{3}LO [39, 40]. Recently the NN potentials up to the fifth oder (N^{4}LO) in the chiral expansion, based on the improved regularization framework have been presented [41, 42]. These chiral NN potentials offer an excellent description of the NN data and provide a solid basis for few-body calculations.

In this paper we present a complete set of deuteron analyzing powers for elastic deuteron–proton (dp) scattering newly obtained with the 186.6 MeV/nucleon (MeV/N) polarized deuteron beam at the RIKEN RI Beam Factory (RIBF). This measurement is a part of the systematic studies of the deuteron analyzing powers for elastic dp scattering at 70–294 MeV/N at the RIBF [13, 16, 18, 33, 43]. In order to clarify the energy dependence the deuteron analyzing powers at 70 and 135 MeV/N previously obtained by us are also shown in the present paper. We compare the data to the theoretical predictions based on the standard NN potentials, namely the CD Bonn, the AV18, the Nijmegen 1 and 2, alone or combined with the commonly used $3N$F models, the TM99 or the Urbana IX. In addition to these spin observables we compare theoretical calculations to Nd elastic scattering cross section data measured previously at 70, 135, and 190 MeV/N by us and the others. To reveal similarities and to find differences between the standard and chiral NN potentials, we compare previously mentioned predictions with the results based on the improved, locally regularized N^{4}LO NN potential of Refs. [41, 42]. The availability of these theoretical predictions in successive orders of chiral expansion up to N^{4}LO allows us to calculate theoretical uncertainties for each observable due to a truncation to a particular order of chiral expansion. Based on that we can indicate the order of chiral expansion required to interpret the Nd scattering data with a sufficient precision.

In Sec. II we shortly describe the experimental procedure and the data analysis. A brief description of the theoretical formalism and forces used in the calculations is given in Sec. III. In Sec. IV the theoretical predictions are compared with the data. Finally in Sec. V we summarize and conclude.

II. EXPERIMENTAL PROCEDURE AND DATA ANALYSIS

A measurement of a complete set of the deuteron analyzing powers for elastic dp scattering at the deuteron laboratory energy of 373.2 MeV (186.6 MeV/N) was performed with the BigDpol system at the RIBF. Only the main features of the experimental procedure and data analysis are briefly summarized in the following; the detailed description can be found in Refs. [33, 43].

The vector and tensor polarized deuteron beams provided by the polarized ion source [44] were first accelerated by the injector cyclotrons AVF and RRC up to 70 MeV/N, and then up to 186.6 MeV/N by the superconducting cyclotron SRC. The BigDpol, located at the extraction beam line of the SRC, consisted of the target chamber, the aluminum cone window and the detector holders. The deuteron beams of intensities of 4-8 nA bombarded a polyethylene (CH_2) target with a thickness of 330 mg/cm^2, placed in the scattering chamber. The four pairs of plastic scintillation counters coupled with photo-multiplier tubes were mounted in two independent planes perpendicular to each other. The opening angle of the BigDpol was 7°–70° in the laboratory system. The scattered deuterons and recoil

protons were detected under a kinematical coincidence condition by each pair of the detectors, which was essential to discriminate the elastic *dp* scattering events from events produced by other scattering processes. The solid angles were determined by the proton detectors with the angular range $\Delta\theta_{\rm lab.} = \pm 1^\circ$. The deuteron beam was stopped in a Faraday cup placed at the focal plane F0 of the BigRIPS spectrometer [45].

The data were taken with polarized and unpolarized beams and the following pairs of the vector, p_Z, and tensor, p_{ZZ}, polarizations were applied (in terms of the theoretical maximum values): $(p_Z, p_{ZZ}) = (0, 0)$, $(1/3, -1)$, $(-2/3, 0)$, and $(1/3, 1)$. The polarizations were changed cyclically at intervals of 5 seconds by switching the RF transition units of the polarized ion source. The beam polarizations were monitored continuously with the beam line polarimeter Dpol using elastic *dp* scattering at 70 MeV/N [46]. At the RIBF the single-turn extractions were available for all the cyclotrons used. Therefore depolarizations were expected to be small during beam acceleration. In the present measurement the beam polarizations achieved 60–70% of the theoretical maximum values.

The analyzing powers iT_{11}, T_{20}, and T_{22} were measured simultaneously with the deuteron spin normal to the horizontal plane. For the T_{21} measurement the spin symmetry axis was rotated in the horizontal plane and aligned at an angle $\beta = 45.0^\circ \pm 1.1^\circ$ with respect to the beam direction. In this experiment the polarization axis of the deuteron beam was rotated with a Wien filter system prior to acceleration [47].

An identification of the scattered deuterons and recoil protons for *dp* elastic scattering events was performed by using the light outputs in the scintillation detectors. Accidental coincidences were estimated by coincidence triggering between adjacent beam bunches. After subtracting accidental coincidences peaks from *dp* elastic scattering were clearly identified both for the deuteron and proton detectors. The effects of the backgrounds other than accidental coincidences, for example events due to the proton knock-out reaction and those from the deuteron breakup reaction, were estimated by changing the integration range of a peak of elastic *dp* scattering for the deuteron and proton detectors, respectively. The results for the analyzing powers changed by 0.005 or less.

The experimental results for the deuteron analyzing powers are shown as (black) circles in the panels e), f) of Figs. 1–4 and are listed in Table I. In the figures only statistical uncertainties are shown. Their values are less than 0.02, 0.02, 0.02, and 0.01 for iT_{11}, T_{20}, T_{21}, and T_{22}, respectively. The uncertainty of the deuteron beam polarization is less than 4%. The uncertainties from the background events do not override the statistical ones.

III. THEORETICAL FORMALISM AND DYNAMICAL INPUTS

Nd scattering with nucleons interacting through a NN potential and through a 3NF is described in terms of a $3N$ scattering operator T which satisfies the Faddeev-type integral equation [1, 48, 49]. We refer to [1, 49, 50] for a general overview of $3N$ scattering and for details on the practical implementation of the Faddeev equations.

We solved the $3N$ Faddeev equation in a partial wave momentum-space basis for three values of the incoming nucleon laboratory energy $E = 70, 135$ and 190 MeV. As a NN interaction we used the high precision semi-phenomenological AV18, CD Bonn, Nijmegen 1 and 2 potentials. We took these interactions alone or together with the TM99 3NF. In the latter case for each NN potential separately the Λ cut-off parameter of the TM99 $3N$ force was adjusted so that this particular combination of a NN- and $3N$-force reproduced the experimental triton binding energy [12]. The AV18 potential was also combined with the Urbana IX 3NF. All these combinations allowed us to find not only the magnitude of 3NF effects but also their dependence on a specific model of the nuclear interactions.

We solved the 3N Faddeev equation also with the locally regularized chiral NN interactions of Refs. [41, 42]. These new NN chiral forces were constructed up to N^{4}LO order of chiral expansion and employ a regularization scheme in the coordinate space using the local regulator $f(r) = [1 - \exp(-r^2/R^2)]^6$ with the regulator parameter $R = 0.8, 0.9, 1.0, 1.1$, and 1.2 fm. Such a regularization led, in particular, to a significant reduction of finite-cutoff artifacts [41, 42, 51] observed for the older versions of the chiral potentials [36, 37]. In the present calculations we used the regulator $R = 0.9$ fm which yields the best description of the NN data. Solutions of the 3N Faddeev equation for the consecutive orders, from LO to N^{4}LO, allowed us to estimate the theoretical uncertainty for various observables calculated at different chiral orders bound with a truncation of chiral expansion to a particular order, according to procedure described in [52].

When solving the $3N$ Faddeev equation we included all 3N partial wave states with a total two-nucleon angular momentum $j \leq 5$ and the total $3N$ angular momentum $J \leq 25/2$.

IV. COMPARISON OF DATA WITH THEORETICAL PREDICTIONS

We show our new data set of the deuteron analyzing powers at 186.6 MeV/N in the panels e), f) of Figs. 1–4 as (black) circles. In these figures also the deuteron analyzing powers taken at 200 MeV/N from Ref. [26] are shown by (orange) x-es. Generally our new data at 186.6 MeV/N agree quite well with the data at 200 MeV/N for the

analyzing powers iT_{11}, T_{20}, and T_{21}, while a rather large difference is found at the forward angles $\theta_{\rm c.m.} \lesssim 60^\circ$ for the tensor analyzing power T_{22}.

In the panels e) of Figs. 1–4 the data sets are compared to the 190 MeV/N theoretical predictions based on the semi-phenomenological standard NN potentials alone or combined with the TM99 3NF. The (blue) dark shaded bands cover the predictions of AV18, CD Bonn, Nijmegen 1 and Nijmegen 2 potentials and the (red) light shaded bands cover the corresponding predictions when the TM99 3NF is included in the calculations. Also the results for the AV18+Urbana IX combination are shown by (black) dashed curves. The (green) solid curves represent the predictions of the locally regularized N^{4}LO chiral potential with regulator $R = 0.9$ fm.

Comparing the standard NN and NN+3NF predictions one finds that at 190 MeV/N quite large effects of the TM99 and Urbana IX 3NF's are visible for iT_{11}, T_{21}, and T_{22} while for T_{20} the predicted 3NF effects are rather small. These effects are localized in the region of the c.m. scattering angles $\theta_{\rm c.m.} \gtrsim 80^\circ$ where large 3NF effects are also predicted for the elastic scattering cross section (see Fig. 5e)). Generally the magnitudes of predicted 3NF effects for the TM99 and Urbana IX are similar. The largest model dependence is seen in the tensor analyzing power T_{21} (see Fig. 3e)). Namely for T_{21} taking the AV18 NN potential and replacing TM99 by Urbana IX 3NF leads to quite different results at the angles $80^\circ \lesssim \theta_{\rm c.m.} \lesssim 160^\circ$. These features may come from the inconsistency of applied 2N- and 3N-forces which are derived independently using different theoretical approaches. This should be improved in future by using consistent NN and 3N forces constructed in the framework of chiral EFT. We see that some of the predicted 3NF effects are supported by the data. For iT_{11} the data roughly support the predicted effects both for the TM99 and the Urbana IX 3NF's. However, this is not the case for T_{21} and T_{22}. For T_{22} the inclusion of the TM99 and the Urbana IX 3NF's improve the description of the data at angles $\theta_{\rm c.m.} \gtrsim 90^\circ$ while at the smaller angles ($\theta_{\rm c.m.} \lesssim 80^\circ$) the data for T_{22} are closer to the calculations based on the pure NN potentials. For T_{21} the smaller Urbana IX 3NF effects at angles $\theta_{\rm c.m.} \gtrsim 90^\circ$ are preferred by data in contrast to the larger effects of the TM99 3NF. For T_{20} the theoretical predictions agree well with the data except for the backward angles $110^\circ \lesssim \theta_{\rm c.m.} \lesssim 150^\circ$, where the data are clearly underestimated by all the calculations, both without and with 3NFs.

Comparing results of calculations employing the chiral NN potential with those of the standard NN potentials, one finds that they provide similar results for T_{20} and T_{22} (see Fig. 2 e) and Fig. 4 e)). These features are the same for the cross section (see Fig. 5e)). For the analyzing powers iT_{11} and T_{21} (see Fig. 1e) and Fig. 3e)) the results are significantly different at the angles around $\theta_{\rm c.m.} = 110^\circ$, where the chiral predictions lie above semi-phenomenological potential results, coming closer to the NN+TM99 predictions.

The complete set of all the deuteron analyzing powers was measured at RIKEN at incident energies from 70 MeV/N up to 294 MeV/N, allowing us to investigate how the picture changes with energy. In the panels a)–d) of Figs. 1–4 we show the data and theoretical results at two other energies: 70 MeV/N and 135 MeV/N. As for 135 MeV/N, the data from Ref. [26] are also presented - they agree quite well with our data. At 70 MeV/N (the panels a) of Figs. 1–4), where effects of a 3NF become visible in elastic scattering cross section (Fig. 5a)), only small 3NF effects are predicted for iT_{11} (Fig. 1a)) and T_{20} (Fig. 2a)). All the theoretical predictions generally follow the experimental data. As for T_{21} (Fig. 3a)) and T_{22} (Fig. 4a)) moderate 3NF effects are seen and the data prefer rather Urbana IX 3NF than TM99 model. The 3NF effects become generally larger for the cross section and analyzing powers for the higher energy of 135 MeV/N (the panels c) of Figs. 1-5). For iT_{11} and T_{20} they are supported by the data both for the TM99 and the Urbana IX 3NF's. For T_{21} the data seem to favour again the Urbana IX 3NF. For T_{22} the picture is unclear. Inclusion of the 3NF's shifts the predictions even further away from the data at the scattering angles around $60^\circ \lesssim \theta_{\rm c.m.} \lesssim 120^\circ$. Going to even larger energies than 190 MeV/N, namely 250 MeV/N and 294 MeV/N, basically gives the similar patterns as those obtained at 190 MeV/N [33]. It should be noted that at the two highest energies large differences between the data and any theoretical calculations are more pronounced for almost all the observables at the very backward angles $\theta_{\rm c.m.} \gtrsim 120^\circ$ [33]. We would also like to stress out that the discrepancies between cross section data and theory seen in the panels a)–d) of Fig. 5 for angles $\theta_{\rm c.m.} \lesssim 30^\circ$ are due to pp Coulomb force [53] omitted in our calculations.

The N^{4}LO chiral potential predictions are close to semi-phenomenological NN results at 70 MeV and 135 MeV for the cross section, iT_{11}, T_{20} and T_{22} but differ in the case of T_{21}. At higher energies N^{4}LO NN predictions are generally away from the data. That would indicate effects of 3NF contributions neglected in our calculations, which grow with the incident energy.

We estimated theoretical truncation uncertainties of our locally regularized chiral NN force predictions at different orders of chiral expansion using the procedure described in Ref. [52] and the scale parameter $\Lambda_b = 600$ MeV. The bands of different colors and decreasing width in the panels b), d), f) of Figs. 1–5 show these theoretical uncertainties, starting from NLO, through N^{2}LO, N^{3}LO up to N^{4}LO. It is clear that the width of estimated error band at N^{4}LO is the smallest for each observable and energy. That width grows with the increasing incident energy and its magnitude allows one to expect that N^{4}LO calculations can describe Nd scattering observables with sufficient accuracy up to energies of ≈ 200 MeV. One also finds that for N^{2}LO the truncation errors are of the order of the discrepancy between N^{4}LO predictions and the data. Since our chiral calculations neglect chiral 3NF's, which for the first time appear at

N^{2}LO, one can expect that those discrepancies can be probably explained when omitted chiral 3NF's are included in future calculations.

V. SUMMARY AND CONCLUSIONS

We have reported a complete set of high precision data for the deuteron analyzing powers iT_{11}, T_{20}, T_{21}, and T_{22}, in elastic dp scattering at 186.6 MeV/nucleon, taken in a wide angular range $39^\circ \leq \theta_{\rm c.m.} \leq 165^\circ$. For all the deuteron analyzing powers the statistical uncertainties are smaller than 0.02 and the systematic uncertainties do not exceed the statistical ones. These data together with our previously reported deuteron analyzing powers taken at different energies constitute a solid basis to guide theoretical investigations of 3NFs.

Our new deuteron analyzing powers and the previously measured data at 70 and 135 MeV/nucleon together with the elastic cross section data in the energy region of interest, are compared with the results of 3N Faddeev calculations based on the standard NN potentials alone or combined with the TM99 3NF. The AV18 NN potential is also combined with the Urbana IX 3NF.

Clear discrepancies between theory restricted to the standard NN potentials and the data have been found at the angles $\theta_{\rm c.m.} \gtrsim 80^\circ$ especially for the deuteron analyzing powers iT_{11} and T_{22} as well as for the differential cross section. The observed discrepancies indicate large 3NF effects for these observables. The predicted 3NF effects grow with the increasing incident energy. The TM99 and the Urbana IX 3NFs give similar effects for almost all the studied observables except for the tensor analyzing power T_{21}, where the stronger dependence on the 3NF model has been found. However the experimental data are not always explained by the calculations with the 3NFs, confirming complex pattern of the 3NF effects in spin observables. These results indicate that one needs additional components of 3NFs other than those of 2π-exchange nature. The observed model dependence of the spin observables calls for using consistent $2N$- and $3N$-forces in a theoretical analysis.

In order to see how the chiral NN forces describe the elastic Nd scattering, the calculations based on the locally regularized N^{4}LO NN potential are shown and compared with the data. Generally the presented calculations based on the chiral N^{4}LO NN potential yield similar predictions to the standard NN potentials for the cross section as well as for the deuteron analyzing powers. However, at higher energies the chiral N^{4}LO results differ significantly from other predictions for iT_{11}, T_{21}, and T_{22}. Estimated theoretical truncation errors at different orders of chiral expansion decrease rapidly with the increasing order, what allows us to conclude that N^{4}LO chiral calculations posses sufficient precision to describe Nd scattering observables. The deviation of such predictions from the data has the same order of magnitude as the theoretical uncertainty of chiral calculations at N^{2}LO. Since at that order a 3NF appears for the first time, it supports additionally the conclusion, that the discrepancies between pure pairwise theory and the data found by us could be probably explained by including chiral 3NF's in our calculations. That conclusion must be verified in future calculations, when consistent $2N$- and $3N$-forces up to at least N^{3}LO are applied.

Acknowledgments

This experiment was performed at RI Beam Factory operated by RIKEN Nishina Center and CNS, University of Tokyo. This work was supported financially in part by the Grants-in-Aid for Scientific Research Numbers 20684010, 24684013 and 16H02171 of the Ministry of Education, Culture, Sports, Science, and Technology of Japan. It was also partially supported by the Polish National Science Center under Grant No's. DEC2013/10/M/ST2/00420 and 2016/22/M/ST2/00173, and by the Japan Society for Promotion of Science (JSPS ID No. S-16020). The numerical calculations were performed on the supercomputer cluster of the JSC, Jülich, Germany.

[1] W. Glöckle, H. Witała, D. Hüber, H. Kamada and J. Golak, Phys. Rep. **274**, 107 (1996).
[2] H.-W. Hammer, A. Nogga, A. Schwenk, Reviews of Modern Physics **85** 197 (2013), and references therein.
[3] N. Kalantar-Nayestanaki *et al.*, Rep. Prog. Phys. **75**, 016301 (2012).
[4] R.B. Wiringa, V.G.J. Stoks, R. Schiavilla, Phys. Rev. C**51**, 38 (1995).
[5] R. Machleidt, Phys. Rev. C**63**, 024001 (2001).
[6] V.G.J. Stoks, R.A.M. Klomp, C.P.F. Terheggen, J.J. de Swart, Phys. Rev. C**49**, 2950 (1994).
[7] S. A. Coon, H.K. Han, Few Body Syst., **30**, 131 (2001).
[8] B. S. Pudliner *et al.*, Phys. Rev. C**56**, 1720 (1997).
[9] H. Witała *et al.*, Phys. Rev. Lett. **81**, 1183 (1998).
[10] W.P. Abfalterer et al., Phys. Rev. Lett. **81**, 57 (1998).

[11] H.Witała, H. Kamada, A. Nogga, W.Glöckle, Ch. Elster, D. Hüber, Phys. Rev. C**59**, 3035 (1999).
[12] H.Witała et al., Phys. Rev. C**63**, 024007 (2001).
[13] N. Sakamoto *et al.*, Phys. Lett. B **367**, 60 (1996).
[14] E. J. Stephenson *et al.*, Phys. Rev. C **60**, 061001 (1999).
[15] R. Bieber *et al.*, Phys. Rev. Lett. **84**, 606 (2000).
[16] H. Sakai *et al.*, Phys. Rev. Lett. **84**, 5288 (2000).
[17] K. Ermisch *et al.*, Phys. Rev. Lett. **86**, 5862 (2001).
[18] K. Sekiguchi *et al.*, Phys. Rev. C **65**, 034003 (2002).
[19] K. Hatanaka *et al.*, Phys. Rev. C **66**, 044002 (2002).
[20] K. Sekiguchi *et al.*, Phys. Rev. C **70**, 014001 (2004).
[21] H. O. Meyer *et al.*, Phys. Rev. Lett. **93**, 112502 (2004).
[22] K. Ermisch *et al.*, Phys. Rev. C **71**, 064004 (2005).
[23] K. Sekiguchi *et al.*, Phys. Rev. Lett. **95**, 0162301 (2005).
[24] St. Kistryn *et al.*, Phys. Rev. C **72**, 044006 (2005).
[25] P. Mermod *et al.*, Phys. Rev. 72, 061002(R) (2005).
[26] B. v. Przewoski *et al.*, Phys. Rev. C **74**, 064003 (2006).
[27] Y. Maeda *et al.*, Phys. Rev. C **76**, 014004 (2007).
[28] H. R. Amir-Ahmadi *et al.*, Phys. Rev. C **75**, 041001 (2007).
[29] A. Ramazani-Moghaddam-Arani *et al.*, Phys. Rev. C **78**, 014006 (2008).
[30] K. Sekiguchi *et al.*, Phys. Rev. C **79**, 054008 (2009).
[31] H. Mardanpour *et al.*, Phys. Lett. B 687, 149 (2010).
[32] K. Sagara, Few Body Syst. **48**, 59 (2010).
[33] K. Sekiguchi *et al.*, Phys. Rev. C **89**, 064007 (2014).
[34] H. Witała, J. Golak, W. Glöckle, H. Kamada, Phys. Rev. **C71**, 054001 (2005).
[35] H. Witała *et al.*, Phys. Rev. C **77**, 034004 (2008).
[36] E. Epelbaum, Prog. Part. Nucl. Phys. **57**, 654 (2006).
[37] R. Machleidt, D. R. Entem, Phys. Rep. **503**, 1 (2011).
[38] E. Epelbaum et al., Phys. Rev. C **66**, 064001 (2002).
[39] V. Bernard, E. Epelbaum, H. Krebs, and U.-G. Meißner, Phys. Rev. C **77**, 064004 (2008).
[40] V. Bernard, E. Epelbaum, H. Krebs, and U.-G. Meißner, Phys. Rev. C**84**, 054001 (2011).
[41] E. Epelbaum, H. Krebs and U.-G. Meißner, Eur. Phys. J. A **51**, no. 5, 53 (2015).
[42] E. Epelbaum, H. Krebs and U.-G. Meißner, Phys. Rev. Lett. **115**, 122301 (2015).
[43] K. Sekiguchi *et al.*, Phys. Rev. C **83**, 061001(R) (2011).
[44] H. Okamura *et al.*, AIP Conf. Proc. **293**, 84 (1994).
[45] T. Kubo *et al.*, Prog. Theor. Exp. Phys. 2012, 03C003 (2012).
[46] K. Suda et al.: Nucl. Instrum. Methods Phys. Res. A. **572**, 745 (2007).
[47] H. Okamura *et al.*, AIP Conf. Proc. **343**, 123 (1995).
[48] H. Witała, T. Cornelius and W. Glöckle, Few-Body Syst. **3**, 123 (1988).
[49] D. Hüber, H. Kamada, H. Witała, and W. Glöckle, Acta Physica Polonica **B28**, 1677 (1997).
[50] W. Glöckle, The Quantum Mechanical Few-Body Problem, Springer-Verlag 1983.
[51] H. Witała, J. Golak, R. Skibiński, and K. Topolnicki, J. Phys. G: Nucl. Part. Phys. **41**, 094011 (2014).
[52] S. Binder *et al.*, Phys. Rev. C **93**, 044002 (2016).
[53] A. Deltuva, A.C. Fonseca, P.U.Sauer, Phys. Rev. C **72**, 054004 (2005).
[54] K. Ermisch *et al.*, Phys. Rev. C **71**, 064004 (2005).
[55] G. Igo *et al.*, Nucl. Phys. A **195**, 33 (1972).
[56] R. E. Adelberger and C. N. Brown, Phys. Rev. D **5**, 2139 (1972).

TABLE I: Data table for all deuteron analyzing powers in dp elastic scattering at the deuteron laboratory energy of 373.2 MeV (186.6 MeV/nucleon) together with the statistical uncertainties.

$\theta_{\mathrm{c.m.}}$(deg)	iT_{11}	ΔiT_{11}	T_{20}	ΔT_{20}	T_{21}	ΔT_{21}	T_{22}	ΔT_{22}
38.9	0.304	0.004	0.024	0.008	—	—	−0.181	0.003
43.7	0.236	0.004	0.029	0.009	−0.032	0.007	−0.211	0.004
48.4	0.142	0.004	0.062	0.010	—	—	−0.250	0.004
54.1	0.025	0.004	0.090	0.011	−0.045	0.004	−0.274	0.004
58.9	−0.061	0.004	0.121	0.014	—	—	−0.302	0.006
63.7	−0.127	0.004	0.137	0.012	−0.114	0.004	−0.324	0.005
68.6	−0.197	0.005	0.151	0.016	−0.159	0.007	−0.335	0.006
73.4	−0.224	0.006	0.109	0.023	−0.198	0.005	−0.331	0.009
78.4	−0.260	0.007	0.104	0.015	−0.232	0.007	−0.335	0.006
83.3	−0.269	0.003	0.083	0.015	—	—	−0.309	0.006
88.3	−0.289	0.006	0.055	0.013	−0.283	0.007	−0.284	0.005
98.4	−0.274	0.007	−0.008	0.013	−0.282	0.004	−0.226	0.005
103.5	−0.260	0.008	−0.015	0.014	−0.270	0.011	−0.197	0.006
108.6	−0.256	0.006	−0.020	0.012	−0.245	0.006	−0.172	0.005
113.8	−0.239	0.005	0.035	0.009	−0.231	0.008	−0.163	0.004
119.0	−0.238	0.013	0.025	0.017	−0.250	0.011	−0.146	0.007
124.2	−0.207	0.004	−0.013	0.008	−0.285	0.007	−0.142	0.003
128.4	−0.187	0.012	−0.054	0.019	−0.310	0.007	−0.148	0.008
133.7	−0.146	0.006	−0.122	0.012	−0.348	0.007	−0.146	0.005
139.0	−0.099	0.006	−0.179	0.012	−0.373	0.007	−0.149	0.005
143.3	−0.053	0.006	−0.216	0.012	−0.420	0.009	−0.152	0.005
148.6	0.012	0.006	−0.277	0.011	−0.446	0.008	−0.171	0.004
154.0	0.077	0.006	−0.330	0.012	−0.484	0.011	−0.178	0.005
158.3	0.102	0.007	−0.379	0.013	−0.494	0.006	−0.177	0.005
161.6	0.124	0.006	−0.443	0.013	−0.479	0.010	−0.155	0.005
164.8	0.138	0.008	−0.468	0.015	—	—	−0.127	0.006

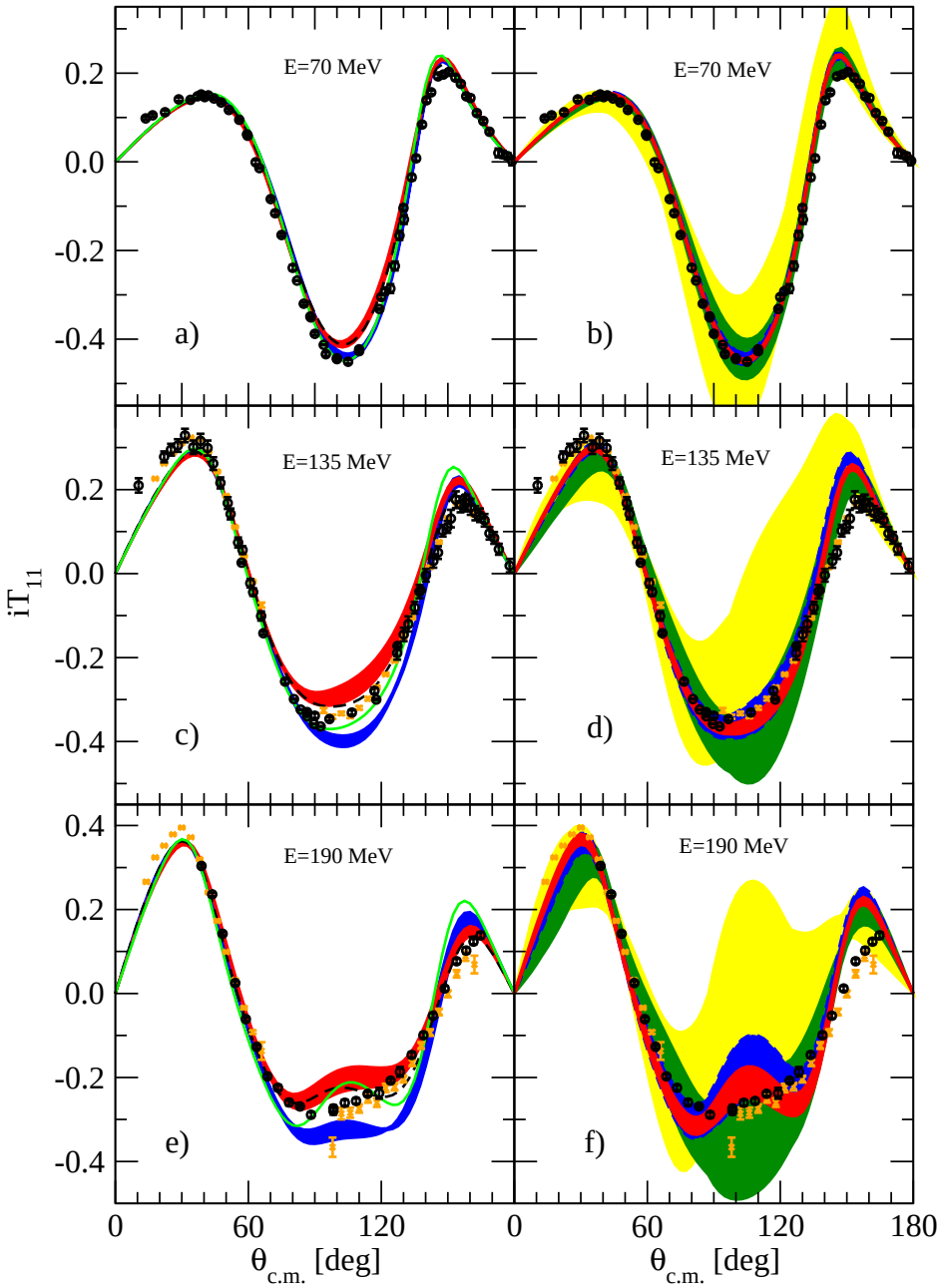

FIG. 1: (color online) The elastic Nd scattering deuteron vector analyzing power iT_{11} at the incoming nucleon laboratory energies $E = 70$ MeV: a) and b), 135 MeV: c) and d), and 190 MeV: e) and f). In a), c), and e) the dark shaded (blue) band covers predictions of standard NN potentials: the AV18, the CD Bonn, Nijmegen 1 and 2 alone and the light shaded (red) band when they are combined with the TM99 3NF. The dashed (black) curve represents the prediction of the AV18+Urbana IX combination. The solid (green) curve shows prediction of the locally regularized (regulator $R = 0.9$ fm) N^{4}LO chiral potential. In b), d), and f) the estimated theoretical uncertainties at different order of chiral expansion are shown by the bands of increasing width at: N^{4}LO (red), N^{3}LO (blue), N^{2}LO (green), and NLO (yellow). The (black) circles are dp data: in a) and b) from [18, 46], in c) and d) from [13, 16, 18, 46], and in e) and f) our new dp data. The (orange) x-es are pd data : at 135 MeV in c) and d), and 200 MeV in e) and f) from [26].

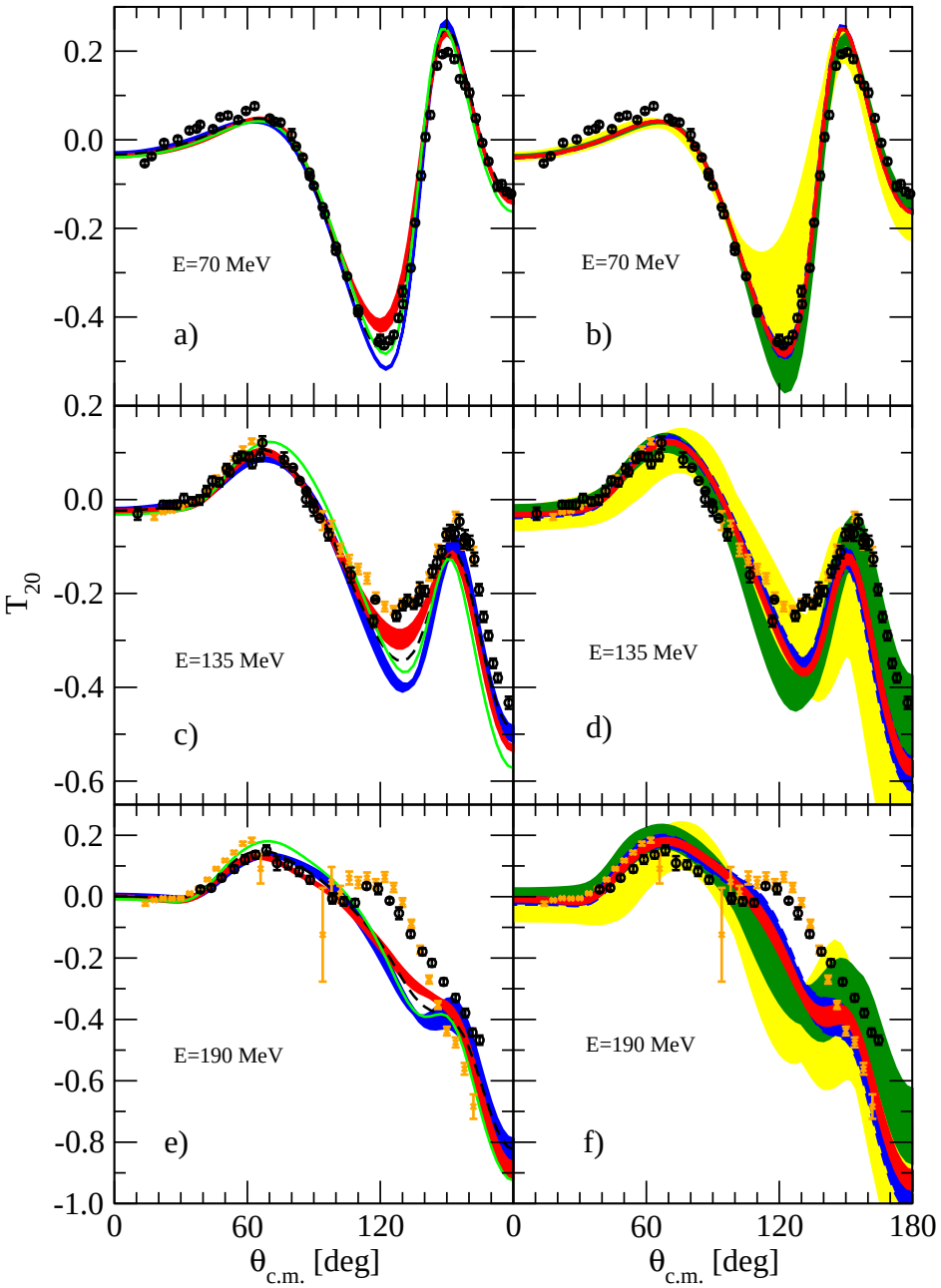

FIG. 2: (color online) The elastic Nd scattering tensor analyzing power T_{20} at the incoming nucleon laboratory energies $E = 70$ MeV: a) and b), 135 MeV: c) and d), and 190 MeV: e) and f). See Fig. 1 for description of bands, curves and data symbols.

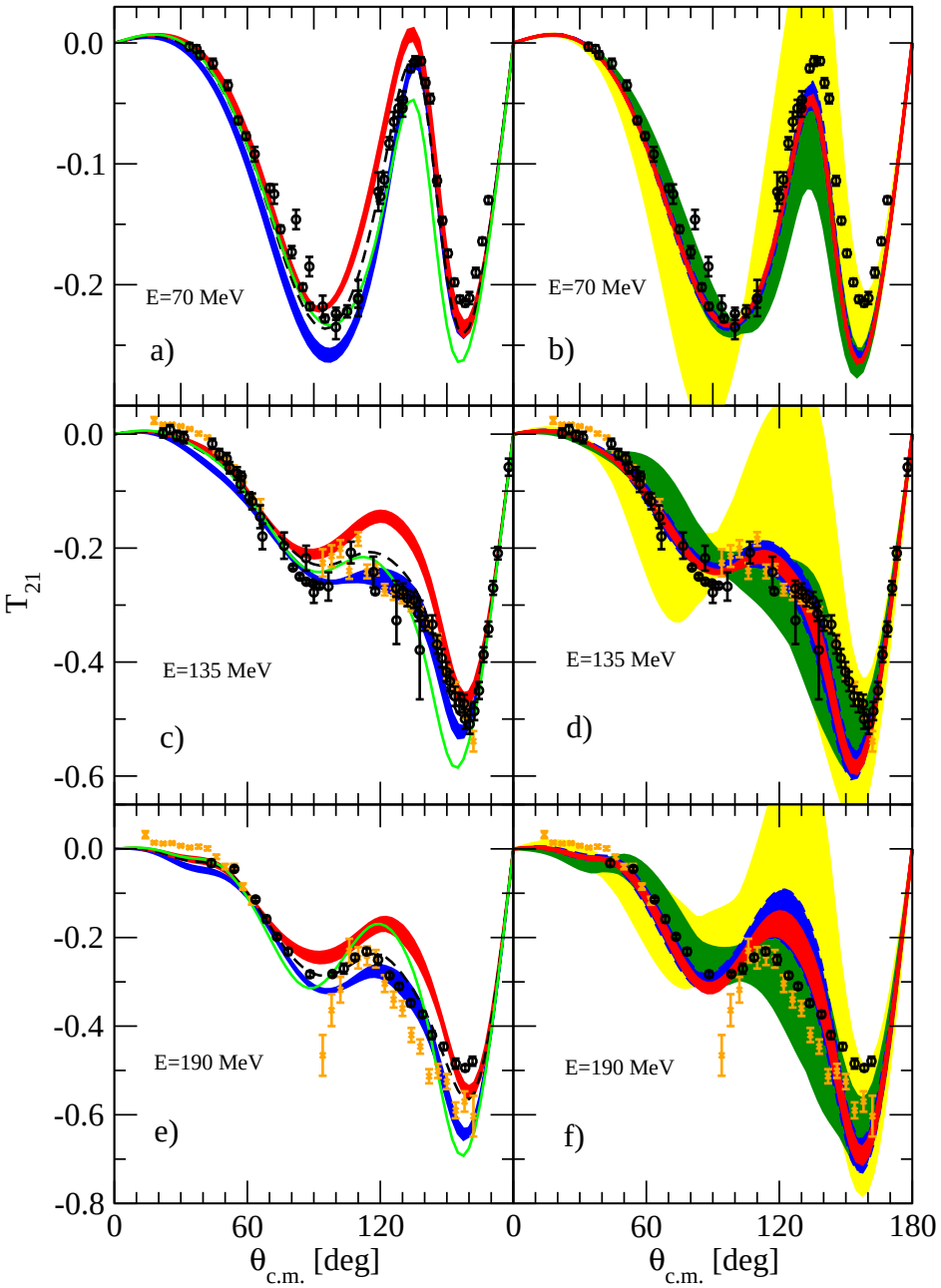

FIG. 3: (color online) The elastic Nd scattering tensor analyzing power T_{21} at the incoming nucleon laboratory energies $E = 70$ MeV: a) and b), 135 MeV: c) and d), and 190 MeV: e) and f). See Fig. 1 for description of bands, curves and data symbols.

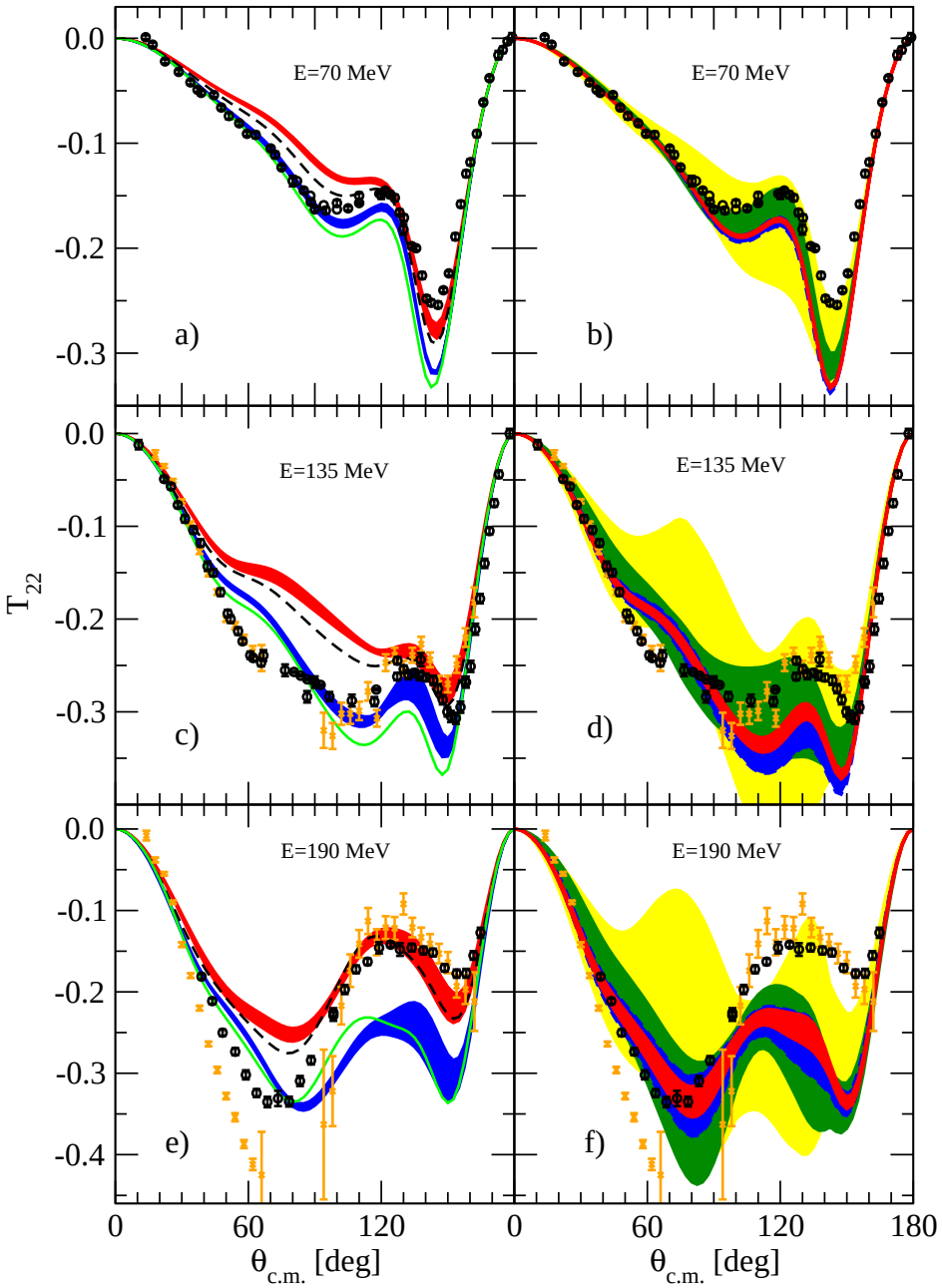

FIG. 4: (color online) The elastic Nd scattering tensor analyzing power T_{22} at the incoming nucleon laboratory energies $E = 70$ MeV: a) and b), 135 MeV: c) and d), and 190 MeV: e) and f). See Fig. 1 for description of bands, curves and data symbols.

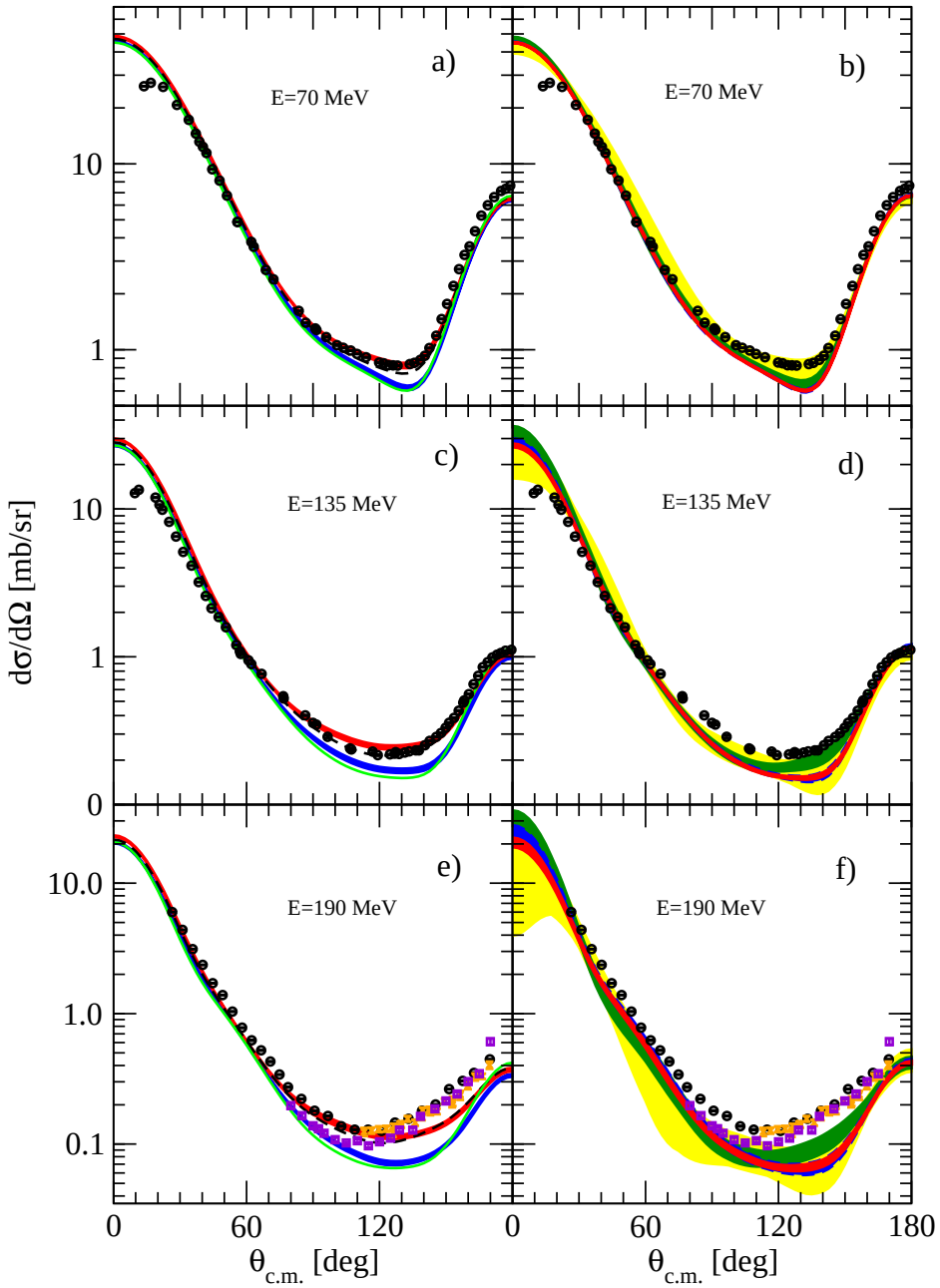

FIG. 5: (color online) The elastic Nd scattering cross section at the incoming nucleon laboratory energies $E = 70$ MeV: a) and b), 135 MeV: c) and d), and 190 MeV: e) and f). The different symbols are dp or pd data: (black) circles in a) and b) from [18], in c) and d) from [13, 16, 18], and in e) and f) from [54]. In e) and f) the (orange) x-es from [55] and the (violet) squares from [56]. See Fig. 1 for description of bands and curves.